ChemPubSoc Europe

DOI: 10.1002/cssc.201700190

CHEMSUSCHEM Communications

Direct Access to Primary Amines and Particle Morphology Control in Nanoporous CO_2 Sorbents

Nesibe A. Dogan[+],[a] Ercan Ozdemir[+],[b] and Cafer T. Yavuz*[a, c]

Chemical tuning of nanoporous, solid sorbents for ideal CO_2 binding requires unhindered amine functional groups on the pore walls. Although common for soluble organics, post-synthetic reduction of nitriles in porous networks often fails due to insufficient and irreversible metal hydride penetration. In this study, a nanoporous network with pendant nitrile groups, microsphere morphology was synthesized in large scale. The hollow microspheres were easily decorated with primary amines through in situ reduction by widely available boranes. The CO_2 capture capacity of the modified sorbent was increased to up to four times that of the starting nanoporous network with a high heat of adsorption (98 kJ mol^{-1}). The surface area can be easily tuned between 1 and 354 m^2 g^{-1}. The average particle size (ca. 50 μm) is also quite suitable for CO_2 capture applications, such as those with fluidized beds requiring spheres of micron sizes.

Elevated CO_2 emissions are a considerable concern due to its environmental impact, whereby increased concentration of CO_2 affects ecological and aquatic systems, resulting in abnormal ocean acidity levels and has direct interferences to human life.[1] One-third of the emissions come from the stationary sources, such as power plants.[2] Efforts to curb levels of CO_2 have led to the development of amine solutions such as monoethanolamine (MEA), as CO_2 is an acidic gas and forms covalent bonds with the basic amine molecules through chemisorption.[3] As CO_2 is bound to amines, chemisorptive processes lead to the formation of carbamate species, which, in turn, yields absorption enthalpies as high as 100 kJ mol^{-1}.[4] This regeneration, particularly the aqueous solution heating and temperature adjustment between cycles brings a significant energy penalty, an undesirable consequence that could constitute up to 70–80% of operating costs or up to 35% loss in energy production.[5]

[a] N. A. Dogan,[+] Prof. C. T. Yavuz
Graduate School of Energy, Environment, Water and Sustainability (EEWS)
Korea Advanced Institute of Science and Technology (KAIST)
34141, Daejeon (Korea)
E-mail: yavuz@kaist.ac.kr

[b] Dr. E. Ozdemir[+]
Institute of Nanotechnology, Gebze Technical University
Cayirova Campus, 41420, Kocaeli (Turkey)

[c] Prof. C. T. Yavuz
Department of Chemistry, KAIST
34141, Daejeon (Korea)

[+] These authors contributed equally to this work.

Supporting Information for this article can be found under: http://dx.doi.org/10.1002/cssc.201700190.

Solid adsorbents with amine functionalities are frequently proposed as alternatives for aqueous amine solutions, as the heat capacities are lower, which would mean lower regeneration costs.[6] Porous materials that allow control over porosity and surface area, such as molecular sieves,[7] mesoporous silica,[8] porous carbons,[7,9] metal–organic frameworks (MOFs),[10] covalent organic polymers, frameworks, or cages[4b,11] and polymers with various linkages and properties,[12] are the most likely classes of solid sorbents to be used in CO_2 capture because of enhanced diffusion during sorption cycles.

Despite their promise in CO_2 capture, porous polymer solids suffer from a number of drawbacks. First and the most evident is their prohibitive cost, mainly because they often require transition metals as building blocks (e.g., in MOFs)[10c] or catalysts in their synthesis (e.g., porous aromatic frameworks (PAFs)).[12f] Secondly, reactive amine sites have to be added post-synthetically because they interfere with the framework construction. Physical impregnation is commonly employed but few studies have successful covalent tethering of amines on the pore walls,[4b,6,12i,13] primarily owing to the inability for reducing agent penetration. A promising direct route, conversion of nitrile into amine, was only successful for a linear, soluble porous polymer.[12j] Post-synthetic conversion of aldehydes into amines has also been reported, whereupon high values for isosteric heat of adsorption (up to 80 kJ mol^{-1}) were observed.[14] In the third and most overlooked setback, the final morphologies of the sorbents are almost always not suitable for deployment in adsorption columns because of their fine powder or crystalline nature.

Herein we report the development of industrially feasible, inexpensive nanoporous network polymers with large spherical bead morphologies (Figure 1). One-pot, metal-free synthesis of hollow polymer beads through suspension polymerization of acrylonitrile (AN) and divinylbenzene (DVB) resulted in materials with surface areas up to 354 m^2 g^{-1} with dominant mesoporosity and well-dispersed nitrile functionalities. Dangling methyl amines were then quantitatively formed by reducing nitriles with boranes and the CO_2 capture capacity was increased to four times that of the original structure.

In a typical synthesis, polymerization starts in a two-phase system and the suspended monomer droplets are converted into cross-linked polymer beads of similar sizes. The water phase, which is also referred to as the continuous phase, contains poly(vinyl alcohol) (PVA) as a stabilizer to reduce the interfacial tension. The organic phase is composed of DVB as cross-linker, 2,2′-azobisisobutyronitrile (AIBN) as radical initiator, AN as monomer, and an organic solvent as porogen. Permanent porosity is introduced with porogens, which is why the

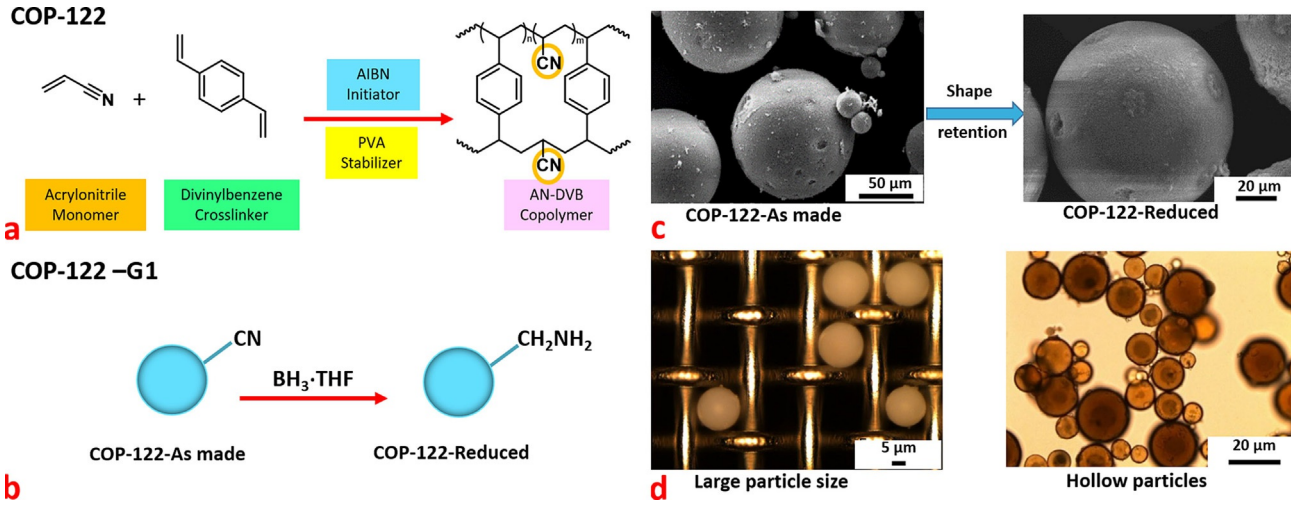

Figure 1. a) Synthesis of acrylonitrile–divinylbenzene copolymer (COP-122) by suspension polymerization. The resulting nanoporous network polymer has the shape of spherical beads with dangling CN groups spread out inside each polymer particle. b) Synthetic pathway to reduce nitrile groups on COP-122. After reduction, amine groups are obtained on polymer surface and inside the pores (COP-122-G1). c) SEM picture of a single polymer particle surrounded by other particles. The morphology of COP-122-G1 is retained after reduction. d) Optical microscope image of COP-122 particles. The large particle size of COP-122 makes it suitable for industrial application.

ratio of porogen to monomer is one of the key factors. Conventional suspension polymerization mechanisms are well known and the factors in controlling microemulsions are formulated elsewhere.[15]

Commonly used volumetric ratios for suspension polymerizations are in the range of 0.1–0.5.[15,16] Here, we kept the ratio of monomer to continuous phase at 0.4 for optimal performance. The organic phase has been introduced into the water phase in a dropwise manner. The resulting polymer was in the form of spherical beads and often had a broad size distribution due to the coalescence and shearing during the polymerization.[17] The synthesized polymer was indexed as covalent organic polymer 122 (COP-122) for easy referral.

In an effort to optimize size and porosity distribution, the effects of the porogen on the final properties of the polymer were investigated. The porogen is an organic solvent, which can also act as a non-solvent. To find out the suitability of common solvents, Kauffman and Jurs used a quantitative structure–property relationship approach for 213 solvents.[18] Polymers formed with different porogens were reported to have similar FTIR spectra. (see the Supporting Information, Figure S13)

The interactions of porogen molecules with each other play a huge role regarding the miscibility of two phases, surface tension, and thermal dissipation in the reaction medium. Viscosity and surface tension are important principles since polymer formation happens due to the existence of two different phases. Thermal conductivity is a crucial parameter, as the porogen molecules travel into and out of the polymer beads, disrupting thermal gradients. Types of solvents and their properties are given in Table S3. For effective comparison, the monomer/porogen ratio was fixed at 1:1 in the organic phase. In this arrangement, 1,4-dioxane gave almost no surface area, 1 $m^2 g^{-1}$, whereas benzene yielded the highest surface area of 354 $m^2 g^{-1}$. Micropore volumes (Table S3) also followed the same trend, benzene having the highest (0.65 $cm^3 g^{-1}$) and 1,4-dioxane the lowest 0.006 $cm^3 g^{-1}$). The reason for this behaviour is related to the surface tension. 1,4-Dioxane has the highest surface tension of all porogens used and, as surface tension is so high, there is not enough time for droplets to form, which leads to very low surface areas. Toluene, mesitylene, and benzene were good porogens for this system, leading to surface areas of 194, 265 and 354 $m^2 g^{-1}$, respectively (Figure S12; full experimental details can be found in the Supporting Information).

To covalently introduce amine groups on COP-122, nitrile functional groups were reduced by borane–tetrahydrofuran complex (BH_3·THF; 1.0 M solution in THF) under N_2 atmosphere. This resulted in complete conversion of the nitril groups into NH_2 groups inside the pores and at the surface of material (Figure 2). This polymer was indexed as COP-122 Generation 1 (COP-122-G1). It is important to note that a variety of metal hydrides or other metal-based hydrogenation routes failed, owing to the irreversible binding of metals to the formed amines and the concomitant clogging of pores. Before the re-

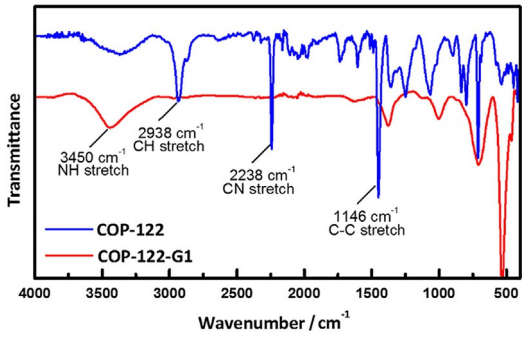

Figure 2. FT-IR spectra of COP-122 (blue) and COP-122-G1 (red). After reduction of the nitrile group in COP-122, the CN stretch at 2238 cm^{-1} had disappeared.

duction (Figure 2, blue line), the spectrum has a strong CN stretching peak at $\tilde{\nu}=2238\ cm^{-1}$, only to disappear completely after the reduction (red line). Instead, a new broad peak of NH stretching at $\tilde{\nu}=3450\ cm^{-1}$ appears, which is a clear sign of the newly formed NH_2 groups. Broad peaks at $\tilde{\nu}=3000$–$3800\ cm^{-1}$ may indicate both OH and NH_2 groups. Reduction of nitrile groups to amino groups is most noticeable by the dramatic increase in the CO_2 uptake. The elemental analysis results for COP-122 before and after the reduction are given in Table S4.

Chemisorption of CO_2 by amine groups is evident in COP-122-G1 (Figure 3, red plot) from the hysteretic type I isotherm that rapidly increases at low partial pressures. The original COP-122 is mainly a physisorptive solid, hence low capacity with negligible hysteresis (Figure 3, blue plot). Conversion of the nitrile groups clearly increases the binding, leading to a dominant chemisorptive mode.

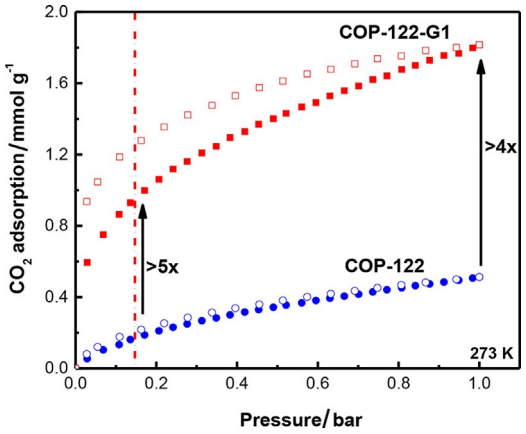

Figure 3. CO_2 adsorption isotherms of COP-122 (blue) and COP-122-G1 (red) at 273 K. By converting nitrile groups into amine groups, CO_2 uptake was increased by a factor of four at 1 bar and 273 K.

The average isosteric heats of adsorption (Q_{st}) for CO_2 in conventional porous solids were reported as 30 and 36 $kJ\,mol^{-1}$ for activated carbon and zeolite 13X, respectively.[19] Lower values of Q_{st} means CO_2 binding is weak and therefore requires less energy for regeneration but at the same time the capture capacity is diminished. Q_{st} values for aqueous amines have been reported to be in excess of 70 $kJ\,mol^{-1}$ up to 84 $kJ\,mol^{-1}$[2] (see comparisons in Table S5). Functional group-dependent variation of Q_{st} was also screened in isostructural POPs. Basic, protic, and bidentate functional groups were found to give the highest values.[20]

The Q_{st} of COP-122 is 53 $kJ\,mol^{-1}$ at zero coverage. Detailed calculations of Q_{st} values (Table S2), fitting isotherms (Figures S1–S5), parameters obtained from fitting by using a dual-site Langmuir–Freundlich model (DSLF; Table S1), and selectivity graphs for ideal adsorbed solution theory (IAST) calculations (Figure S4) are given in the Supporting Information. However, COP-122-G1 exhibits Q_{st} values at 98 $kJ\,mol^{-1}$ at zero coverage that are almost twice as high (Figure S3). These values show the chemisorptive nature of COP-122-G1, which arises from the amine functionalities covalently grafted in the pores.[21]

Following the reduction of nitrile groups to amine groups, the pore-size distributions are also expected to have changed, as these reactions are believed to have occurred inside the pores. From the BET specific surface area and pore-size distribution analysis (Figure S8) by using N_2 probe at 77 K, the surface area was found to have dropped sharply to 38 $m^2\,g^{-1}$ (from 354 $m^2\,g^{-1}$) and pores smaller than 9 nm were completely filled up.

COP-122 was formed as beads and different sized beads were visible under a standard optical microscope (Figure S16). As optical observation suggests, the beads were more transparent inside, having a hollow core/mesoporous shell structure. To our knowledge, no suspension polymerization reaction was previously reported to produce hollow beads. The shell thickness was 0.5–3.5 μm and the total particle diameter was 1–50 μm (Figure S17). SEM images also showed that the particles were spherical in shape and the porous nature inside of the particle was visible at higher magnifications (Figures S16 and S17). All different particles were also shown to be stable in air and N_2 atmospheres (Figures S14 and S15). Reusability tests were carried out and no significant differences were observed after 5 cycles (Figure S11).

In summary, acrylonitrile–divinylbenzene copolymers with nanoporous structure have been designed and synthesized for effective and cheap post-combustion CO_2 capture. The synthesized COP-122 polymer was obtained in the form of spherical beads up to 100 μm in diameter, with hollow core/mesoporous shell structures. Surface areas and pore volumes could be altered by employing different types of porogen and the highest observed surface area was 354 $m^2\,g^{-1}$. The hollow core inside each single particle shows potential for use as a carrier for various cargos, such as drugs. The amine impregnation and functionalization of COP-122 particles make them promising candidates for CO_2 capture operations. Furthermore, this material is easy to handle because of its large particle size and non-corrosive nature, providing low attrition potential.

Experimental Section

Synthesis

AN–DVB beads were synthesized by a pre-polymerization step followed by conventional suspension polymerization. The aqueous phase was prepared at 338 K with poly (vinyl alcohol) (500 mg) in water (50 mL). The solution containing monomers (AN and DVB), porogen, and initiator (AIBN) was sonicated for 10 min to dissolve AIBN completely at room temperature. The sonicated mixture was introduced to the aqueous phase in a dropwise manner. Polymerization was carried out at 348 K over 24 h. After polymerization, the beads were filtered, washed with methanol (2×100 mL), and dried under vacuum. The synthesized polymer is referred to as covalent organic polymer 122 (COP-122). See the Supporting Information for further details.

For the synthesis of COP-122-G1, a suspension of COP-122 (500 mg) in dry tetrahydrofuran (THF; 200 mL) was formed under N_2 atmosphere. A 1.0 M solution of borane–tetrahydrofuran complex (BH_3·THF) in THF (10 mL) was added at room temperature. As

borane complexes are air- and moisture-sensitive, reaction should be carried out in a fume hood and under nitrogen atmosphere. The reaction was continued at 348 K for 12 h. After 12 h, the slurry was taken out, neutralized, and washed with 5% HCl in MeOH (*v/v*, 50 mL), 5 % NaOH in MeOH (*w/v*, 50 mL), and MeOH (50 mL). The solid particles were separated by filtration and dried under vacuum. This product is referred as COP-122-G1. See the Supporting Information for further details.

Calculation of Q_{st} values and IAST selectivity values

Isosteric heats of adsorption as a function of CO_2 loading has been calculated from the CO_2 adsorption data measured at 273 K and 298 K by using the Clausius–Clapeyron equation. CO_2 adsorption isotherms at 273 K and 298 K are given in Figure 3 and Figure S6, respectively. To use the Clausius–Clapeyron equation [Eq. (1)], it is necessary to know how the pressure changes as a function of loading of the gas of interest. P is the pressure, Q_{st} is the heat of adsorption, R is the gas constant, and T is the temperature.

$$\ln\frac{P_1}{P_2} = -\frac{Q_{st}}{R}\left(\frac{1}{T_1}-\frac{1}{T_2}\right) \quad (1)$$

To calculate Q_{st}, values of T and P must be calculated from the experimental data. Data was fitted by using dual-site Langmuir–Freundlich (DSLF) model [Eq. (2)] by using OriginPro 8.5 software,[4b] since this model is known to give a realistic fitting. Here, Q is the absorbed quantity, q_1 and q_2 are the saturated adsorption capacities, p is the pressure, b_1 and b_2 are Langmuir parameter of affinity coefficients associated with the site, and n_1 and n_2 are deviations from an ideal surface.

$$Q = \frac{q_1 \times b_1 \times p^{1/n_1}}{1 + b_1 \times p^{1/n_1}} + \frac{q_2 \times b_2 \times p^{1/n_2}}{1 + b_2 \times p^{1/n_2}} \quad (2)$$

The fitted isotherms are given in Figure S1 and the fitted parameters are presented in Table S1. Adjusted R^2 values for each fit, also shown in Table S1, indicated the goodness of fit for each data set. After these parameters were obtained, pressure values were calculated by using Wolfram Mathematica 9.0.[12a] The obtains isotherms are given in Figure S2 and the Clausius–Clapeyron equation and values are given in Table S2. Finally, the obtained Q_{st} graphs are given in Figure S3. For selectivity calculations, the ideal adsorbed solution theory (IAST) method was employed. To calculate the integrations of this method, data from the single-component experimental CO_2 uptake isotherm was fitted by DSLF model [Eq. (2)] in Wolfram Mathematica 9.0. N_2 uptake isotherms were fitted by single-site Langmuir–Freundlich (SSLF) model. Other models can also be used for fitting, as long as the experimental points are fitted precisely to the calculated fitting line. Selectivity of CO_2 over N_2 predicted by IAST for 15:85 CO_2/N_2 mixtures at 273 K with increasing pressure (bar) is presented in Figure S4 for both COP-122 and COP-122-G1. Isosteres of the Clausius–Clapeyron equation are presented in Figure S5.

Acknowledgements

We acknowledge the financial support of the National Research Foundation of Korea (NRF) by a grant funded by the Korean government (MSIP; No. NRF-2016R1A2B4011027).

Keywords: adsorption · carbon capture · mesoporous materials · porous polymers · postsynthetic modification

[1] a) J. C. Orr, V. J. Fabry, O. Aumont, L. Bopp, S. C. Doney, R. A. Feely, A. Gnanadesikan, N. Gruber, A. Ishida, F. Joos, R. M. Key, K. Lindsay, E. Maier-Reimer, R. Matear, P. Monfray, A. Mouchet, R. G. Najjar, G. K. Plattner, K. B. Rodgers, C. L. Sabine, J. L. Sarmiento, R. Schlitzer, R. D. Slater, I. J. Totterdell, M. F. Weirig, Y. Yamanaka, A. Yool, *Nature* **2005**, *437*, 681–686; b) D. M. D'Alessandro, B. Smit, J. R. Long, *Angew. Chem. Int. Ed.* **2010**, *49*, 6058–6082; *Angew. Chem.* **2010**, *122*, 6194–6219; c) H. A. Patel, C. T. Yavuz, *Faraday Discuss.* **2015**, *183*, 401–412.

[2] S. Choi, J. H. Drese, C. W. Jones, *ChemSusChem* **2009**, *2*, 796–854.

[3] A. Samanta, A. Zhao, G. K. H. Shimizu, P. Sarkar, R. Gupta, *Ind. Eng. Chem. Res.* **2012**, *51*, 1438–1463.

[4] a) R. Vaidhyanathan, S. S. Iremonger, G. K. H. Shimizu, P. G. Boyd, S. Alavi, T. K. Woo, *Science* **2010**, *330*, 650–653; b) D. Thirion, V. Rozyyev, J. Park, J. Byun, Y. Jung, M. Atilhan, C. T. Yavuz, *Phys. Chem. Chem. Phys.* **2016**, *18*, 14177–14181.

[5] a) G. T. Rochelle, *Science* **2009**, *325*, 1652–1654; b) D. Aaron, C. Tsouris, *Sep. Sci. Technol.* **2005**, *40*, 321–348.

[6] T. M. McDonald, J. A. Mason, X. Kong, E. D. Bloch, D. Gygi, A. Dani, V. Crocella, F. Giordanino, S. O. Odoh, W. S. Drisdell, B. Vlaisavljevich, A. L. Dzubak, R. Poloni, S. K. Schnell, N. Planas, K. Lee, T. Pascal, L. F. Wan, D. Prendergast, J. B. Neaton, B. Smit, J. B. Kortright, L. Gagliardi, S. Bordiga, J. A. Reimer, J. R. Long, *Nature* **2015**, *519*, 303–308.

[7] R. V. Siriwardane, M.-S. Shen, E. P. Fisher, J. A. Poston, *Energy Fuels* **2001**, *15*, 279–284.

[8] S. Lee, S.-Y. Moon, H. Kim, J.-S. Bae, E. Jeon, H.-Y. Ahn, J.-W. Park, *RSC Adv.* **2014**, *4*, 1543–1550.

[9] a) J. L. Figueiredo, M. F. R. Pereira, M. M. A. Freitas, J. J. M. Órfão, *Carbon* **1999**, *37*, 1379–1389; b) J. W. F. To, J. He, J. Mei, R. Haghpanah, Z. Chen, T. Kurosawa, S. Chen, W.-G. Bae, L. Pan, J. B. H. Tok, J. Wilcox, Z. Bao, *J. Am. Chem. Soc.* **2016**, *138*, 1001–1009.

[10] a) K. Sumida, D. L. Rogow, J. A. Mason, T. M. McDonald, E. D. Bloch, Z. R. Herm, T.-H. Bae, J. R. Long, *Chem. Rev.* **2012**, *112*, 724–781; b) P. M. Bhatt, Y. Belmabkhout, A. Cadiau, K. Adil, O. Shekhah, A. Shkurenko, L. J. Barbour, M. Eddaoudi, *J. Am. Chem. Soc.* **2016**, *138*, 9301–9307; c) J.-R. Li, R. J. Kuppler, H.-C. Zhou, *Chem. Soc. Rev.* **2009**, *38*, 1477–1504; d) P. K. Thallapally, J. Tian, M. Radha Kishan, C. A. Fernandez, S. J. Dalgarno, P. B. McGrail, J. E. Warren, J. L. Atwood, *J. Am. Chem. Soc.* **2008**, *130*, 16842–16843; e) J. M. Lownsbury, I. A. Santos-López, W. Zhang, C. T. Campbell, H. S. Yu, W.-G. Liu, C. J. Cramer, D. G. Truhlar, T. Wang, J. T. Hupp, O. K. Farha, *J. Phys. Chem. C* **2016**, *120*, 16850–16862.

[11] a) L. Guo, X. Zeng, D. Cao, *Sens. Actuators B* **2016**, *226*, 273–278; b) Y. Zhu, S. Wan, Y. Jin, W. Zhang, *J. Am. Chem. Soc.* **2015**, *137*, 13772–13775; c) O. Buyukcakir, Y. Seo, A. Coskun, *Chem. Mater.* **2015**, *27*, 4149–4155.

[12] a) T. Islamoglu, S. Behera, Z. Kahveci, T.-D. Tessema, P. Jena, H. M. El-Kaderi, *ACS Appl. Mater. Interfaces* **2016**, *8*, 14648–14655; b) A. Thomas, *Angew. Chem. Int. Ed.* **2010**, *49*, 8328–8344; *Angew. Chem.* **2010**, *122*, 8506–8523; c) S. K. Kundu, A. Bhaumik, *ACS Sustainable Chem. Eng.* **2016**, *4*, 3697–3703; d) X. L. Cui, K. J. Chen, H. B. Xing, Q. W. Yang, R. Krishna, Z. B. Bao, H. Wu, W. Zhou, X. L. Dong, Y. Han, B. Li, Q. L. Ren, M. J. Zaworotko, B. L. Chen, *Science* **2016**, *353*, 141–144; e) H. Li, X. Ding, Y.-C. Zhao, B.-H. Han, *Polymer* **2016**, *89*, 112–118; f) T. Ben, H. Ren, S. Ma, D. Cao, J. Lan, X. Jing, W. Wang, J. Xu, F. Deng, J. M. Simmons, S. Qiu, G. Zhu, *Angew. Chem. Int. Ed.* **2009**, *48*, 9457–9460; *Angew. Chem.* **2009**, *121*, 9621–9624; g) C. Gu, N. Huang, Y. Chen, H. Zhang, S. Zhang, F. Li, Y. Ma, D. Jiang, *Angew. Chem. Int. Ed.* **2016**, *55*, 3049–3053; *Angew. Chem.* **2016**, *128*, 3101–3105; h) W. Choi, K. Min, C. Kim, Y. S. Ko, J. W. Jeon, H. Seo, Y.-K. Park, M. Choi, *Nat. Commun.* **2016**, *7*, 12640; i) J. H. Lee, H. J. Lee, S. Y. Lim, B. G. Kim, J. W. Choi, *J. Am. Chem. Soc.* **2015**, *137*, 7210–7216; j) S. Wang, X. Li, H. Wu, Z. Tian, Q. Xin, G. He, D. Peng, S. Chen, Y. Yin, Z. Jiang, M. D. Guiver, *Energy Environ. Sci.* **2016**, *9*, 1863–1890; k) M. Lee, C. G. Bezzu, M. Carta, P. Bernardo, G. Clarizia, J. C. Jansen, N. B. McKeown, *Macromolecules* **2016**, *49*, 4147–4154.

[13] a) M. Gökmen, F. Du Prez, *Prog. Polym. Sci.* **2012**, *37*, 365–405; b) W. Lu, J. P. Sculley, D. Yuan, R. Krishna, Z. Wei, H.-C. Zhou, *Angew. Chem. Int. Ed.* **2012**, *51*, 7480–7484; *Angew. Chem.* **2012**, *124*, 7598–7602; c) L.-B.

Sun, A.-G. Li, X.-D. Liu, X.-Q. Liu, D. Feng, W. Lu, D. Yuan, H.-C. Zhou, *J. Mater. Chem. A* **2015**, *3*, 3252 – 3256; d) A. K. Sekizkardes, J. T. Culp, T. Islamoglu, A. Marti, D. Hopkinson, C. Myers, H. M. El-Kaderi, H. B. Nulwala, *Chem. Commun.* **2015**, *51*, 13393 – 13396; e) L.-B. Sun, Y.-H. Kang, Y.-Q. Shi, Y. Jiang, X.-Q. Liu, *ACS Sustainable Chem. Eng.* **2015**, *3*, 3077 – 3085.

[14] C. Xu, Z. Bacsik, N. Hedin, *J. Mater. Chem. A* **2015**, *3*, 16229 – 16234.

[15] R. Arshady, *Colloid Polym. Sci.* **1992**, *270*, 717 – 732.

[16] a) D. S. S. Nunes, F. M. B. Coutinho, *Eur. Polym. J.* **2002**, *38*, 1159 – 1165; b) M. Kaliva, G. S. Armatas, M. Vamvakaki, *Langmuir* **2012**, *28*, 2690 – 2695.

[17] W.-H. Li, H. D. H. Stöver, *J. Polym. Sci. Part A* **1998**, *36*, 1543 – 1551.

[18] G. W. Kauffman, P. C. Jurs, *J. Chem. Inf. Comput. Sci.* **2001**, *41*, 408 – 418.

[19] C. R. Mason, L. Maynard-Atem, K. W. J. Heard, B. Satilmis, P. M. Budd, K. Friess, M. Lanč, P. Bernardo, G. Clarizia, J. C. Jansen, *Macromolecules* **2014**, *47*, 1021 – 1029.

[20] M. H. Alkordi, R. R. Haikal, Y. S. Hassan, A.-H. Emwas, Y. Belmabkhout, *J. Mater. Chem. A* **2015**, *3*, 22584 – 22590.

[21] H. A. Patel, J. Byun, C. T. Yavuz, *ChemSusChem* **2017**, DOI: 10.1002/cssc.201601545.

Manuscript received: February 3, 2017
Revised: March 13, 2017
Accepted Article published: March 13, 2017
Final Article published: March 29, 2017